5180–5187 *Nucleic Acids Research, 2012, Vol. 40, No. 11* *Published online 9 February 2012*
doi:10.1093/nar/gks142

A tunable zinc finger-based framework for Boolean logic computation in mammalian cells

Jason J. Lohmueller[1,2], Thomas Z. Armel[1] and Pamela A. Silver[1,2,*]

[1]Department of Systems Biology and [2]Wyss Institute for Biologically Inspired Engineering, Harvard University, Boston, MA 02115, USA

Received December 14, 2011; Revised January 19, 2012; Accepted January 20, 2012

ABSTRACT

The ability to perform molecular-level computation in mammalian cells has the potential to enable a new wave of sophisticated cell-based therapies and diagnostics. To this end, we developed a Boolean logic framework utilizing artificial Cys_2–His_2 zinc finger transcription factors (ZF-TFs) as computing elements. Artificial ZFs can be designed to specifically bind different DNA sequences and thus comprise a diverse set of components ideal for the construction of scalable networks. We generate ZF-TF activators and repressors and demonstrate a novel, general method to tune ZF-TF response by fusing ZF-TFs to leucine zipper homodimerization domains. We describe 15 transcriptional activators that display 2- to 463-fold induction and 15 transcriptional repressors that show 1.3- to 16-fold repression. Using these ZF-TFs, we compute OR, NOR, AND and NAND logic, employing hybrid promoters and split intein-mediated protein splicing to integrate signals. The split intein strategy is able to fully reconstitute the ZF-TFs, maintaining them as a uniform set of computing elements. Together, these components comprise a robust platform for building mammalian synthetic gene circuits capable of precisely modulating cellular behavior.

INTRODUCTION

Mammalian synthetic gene circuits have the potential to directly impact human health in applications such as cell- and animal-based disease models, gene therapies and smart therapeutics. Significant progress has been made to generate such networks, including: RNAi-based systems to interrogate siRNAs, microRNAs and synthetic transcription factors, RNA aptamer systems to sense multiple small molecules and metabolites and transcription factor-based systems to sense synthetic small molecules (1–6). However, despite the efficacy of these systems several engineering challenges remain. The majority of published systems rely on the use of a small set of specialized factors such as LacI, Gal4 and TetR and are not amenable to the design of large-scale networks. Methods to tune system responses over a wide dynamic range are lacking and are often specific to specialized system components. Finally, many signal integration strategies are limited by their input modularity and are not amenable to the facile generation of different types of logic gates. In this work, we address these issues by developing a computational platform consisting of Cys_2–His_2 zinc finger transcription factors (ZF-TF) computing elements, general strategies to tune these ZF-TFs and general strategies to integrate transcriptional input signals.

Cys_2–His_2 ZFs are small protein domains sharing a common zinc atom coordinating structural motif, many of which are capable of binding to specific DNA sequences with high affinities. Recent advances in the ability to engineer ZF DNA binding domains (DBDs) to recognize new nucleotide sequences have made them a rich potential source of independently functioning system components (7,8). As most artificial ZFs are constructed from a single canonical ZF, Zif268, they are also similar in amino acid composition and structure and are likely to share similar biological properties. In our systems, we use a set of five previously developed ZF DBDs that target three orthogonal 9 bp DNA sequences with high specificity: BCR_ABL-1, BCR_ABL-2, erbB2, HIV-1 and HIV-2 (9).

Because biological signals vary greatly in strength and composition, it is desirable to have a set of tunable computing elements to interrogate these signals. A common cellular strategy to modulate TF activity is through cooperative binding between TFs, a process often mediated by leucine zipper (LZ) protein–protein interaction domains (10). Whereas the effect of LZs on the structure and function of ZF DBDs has been

*To whom correspondence should be addressed. Tel.: +1 617 432 6401; Fax: +1 617 432 5012; Email: pamela_silver@hms.harvard.edu

The authors wish it to be known that, in their opinion, the first two authors should be regarded as joint First Authors.

characterized biochemically, the use of LZs to modulate ZF-TF activity in cells has not been explored (11–13). We chose two well-characterized homodimerizing LZ domains with different binding affinities, the protein interaction domains of human c-Jun ($K_d = 448\mu M$) and *Saccharomyces cerevisiae* GCN4 ($K_d = 8\,nM$), to tune our engineered ZF-TFs (14,15). We combine and compare this new tuning strategy to a previously shown method to modulate TF activity, altering the number of binding sites in ZF response promoters, further increasing the range of system tunability.

To date, relatively few transcriptional logic gates have been demonstrated, and gates have largely been pursued outside the context of a general computational framework. To compute OR and NOR logic using transcriptional networks, previous researchers have used hybrid transcription factor response promoters containing binding sites for multiple TFs (1). We demonstrate that it is also possible to create and tune ZF-TF-based OR and NOR gates using this architecture. Previous efforts to create individual AND gates have relied on the association of split TF fragments in two-hybrid systems, potentially limiting the activation strength of these systems and scalability (6). To our knowledge, a NAND gate has not been constructed using split transcription factors in mammalian cells.

We chose to pursue split intein-mediated protein splicing as an attractive alternative approach to perform both AND and NAND computations. Split inteins, when fused to separate protein fragments, auto-catalytically splice the two fragments into a single protein without leaving a peptide scar. They have been shown to function at high efficiency in mammalian cells and in a wide range of proteins, and over 500 inteins have been discovered to date (16–18). We chose to use the dnaB mini-intein from *Rhodothermus marinus* as it has been previously demonstrated to display ~100% splicing efficiency in mammalian cells (16). Utilizing this protein splicing strategy we can reconstitute ZF-TFs for AND and NAND gates allowing logic computations to be enacted by complete factors, potentially yielding stronger and more uniform system responses.

MATERIALS AND METHODS

Recombinant DNA constructs

Constructs encoding ZF DBDs were codon-optimized for mammalian expression and synthesized (Genscript). The rma intein fragments and the GCN4 leucine zipper sequences were codon optimized for mammalian expression and synthesized (Integrated DNA Technologies). Intein-ZF fusion parts were cloned using PCR and BbsI Type-IIS restriction enzyme methods. All experimental DNA constructs were generated by combining BioBrick subparts using Biobrick assembly (19,20). Each final construct and its constituent Biobrick subparts is listed in Supplementary Table S1. Sequences of all Biobrick subparts are listed in Supplementary Table S2. For expression constructs, coding regions cut with XbaI and NotI were cloned into the NheI and NotI sites of a modified version of pCDNA5/FRT/TO (Invitrogen), 'pCDNA5insVector'. pCDNA5insVector was generated by cloning the subpart 'pCDNA5ins' between the two PmeI sites of pCDNA5/FRT/TO. All reporter constructs were cut with SpeI and NotI and cloned between the SpeI and NotI sites of pCDNA5/FRT/TO.

Cell culture

The human osteosarcoma-derived epithelial cell line U-2 OS (ATCC no. HTB-96) was maintained at 37°C, 5% CO_2 in growth medium (McCoy's 5A medium supplemented with 10% FBS, 2 mM L-glutamine, 100 U/ml penicillin and 100 µg/ml streptomycin). A summary of the plasmid amounts used for transfections can be found in Supplementary Table S1. All transfections were performed in 12-well plates seeded with ~150 000 cells using 3 µl Lipofectamine LTX transfection reagent and 1 µl PLUS reagent (Invitrogen) with 1 µg total DNA per well in 1 ml of growth medium. Transfection reagent was washed out and replaced with fresh growth media 6 h post-transfection.

Microscopy

Microscopy was performed on live cells in glass-bottomed wells (MatTek) in phenol red-free growth medium 48 h post-transfection. Cells were imaged by a Nikon TE-2000 microscope with a 20× PlanFluor NA = 0.5, DIC M/N2 objective and an ORCA-ER charge-coupled device camera. Data collection and processing were performed using Metamorph 7.0 software (Molecular Devices). All images within a given experimental set were collected using the same exposure times, averaged over three frames and underwent identical processing.

Flow cytometry

Approximately 30 000 live cells from each transfected well were analyzed using an LSRII cell analyser (BD Biosciences) in three biological replicates. Cells were trypsinized with 0.1 ml of 0.25% trypsin–EDTA, pelleted and resuspended in 100 µl of Dulbecco's phosphate buffered saline containing 0.1% FBS. Output was assayed 48 h post-transfection. First, the total AmCyan fluorescent protein (CFP) signal of mCh+ cells was calculated by multiplying the frequency of CFP+ cells in the mCH+ population by the mean CFP signal of these double positive cells. Fold change was calculated by dividing the total CFP of mCH+ experimental cells by the total CFP values of mCH+ off-target control cells. An example of the raw data and gating procedure is given in Supplementary Figure S3. Values were averaged over three replicates and standard deviations were determined. In assays containing multiple off-target experiments, fold changes were calculated using the average of all off-target control wells to compare the background leakiness of the different reporter constructs. Total CFP values and standard deviations for all experiments are listed in Supplementary Table S4.

RESULTS

Tuning ZF-TFs

We first generated a set of 15 ZF transcriptional activators and demonstrated the ability to increase their activity with increasing LZ strength. Each activator was comprised of a ZF DBD, either no LZ motif, a Jun LZ, or a GCN4 LZ, the transcriptional activation domain VP64 and the SV40 nuclear localization signal (NLS). Activators were expressed from the CMV promoter and tagged with co-translationally cleaved t2a:mCherry to monitor expression (Figure 1A) (21). We assayed activator function by co-transfection with reporter plasmids containing different numbers of ZF binding sites driving expression of AmCyan fluorescent protein CFP (Figure 1A). We first tested the BCR_ABL-1 activators and observed a wide range of signal output (2- to 163-fold) that increased with both the strength of the LZ binding domain and the number of ZF binding sites (Figure 1B and Supplementary Figure S2). We then compared the activity of ZF activators generated using different DBDs by co-transfection with the corresponding 6× Binding site (BS) reporter (Figure 1C and Supplementary Figure S3). A strong induction from all ZFs was observed (up to 463-fold), with HIV TFs displaying the strongest activation. No cross-reactivity was observed with activators co-transfected with off-target reporters, demonstrating the specificity of our ZF-TFs (Supplementary Figures S4 and S5).

The modular nature of our ZF elements allowed for the facile construction of a set of transcriptional repressors. These repressors can be tuned by altering the LZ dimerization domain and number of target sites analogous to our ZF activator constructs. We created 15 artificial ZF repressors by combining ZF DBDs, the SV40 NLS and LZs with the Krüppel-associated Box (KRAB) transcriptional repression domain (Figure 2A). To assay for repression, we generated CFP reporter constructs containing variable numbers of copies of a 9 bp ZF binding site directly downstream of the TATA box within the CMV promoter (Figure 2A). We first tested BCR_ABL-1 repressors and observed a significant decrease in output signal (2- to 9-fold), strengthening with the number of ZF binding sites and the presence of a LZ (Figure 2B and Supplementary Figure S6). All ZF repressors were then tested with corresponding 6× reporters, and displayed a similar pattern—higher levels of repression for ZF repressors with a LZ domain (Figure 2C and Supplementary

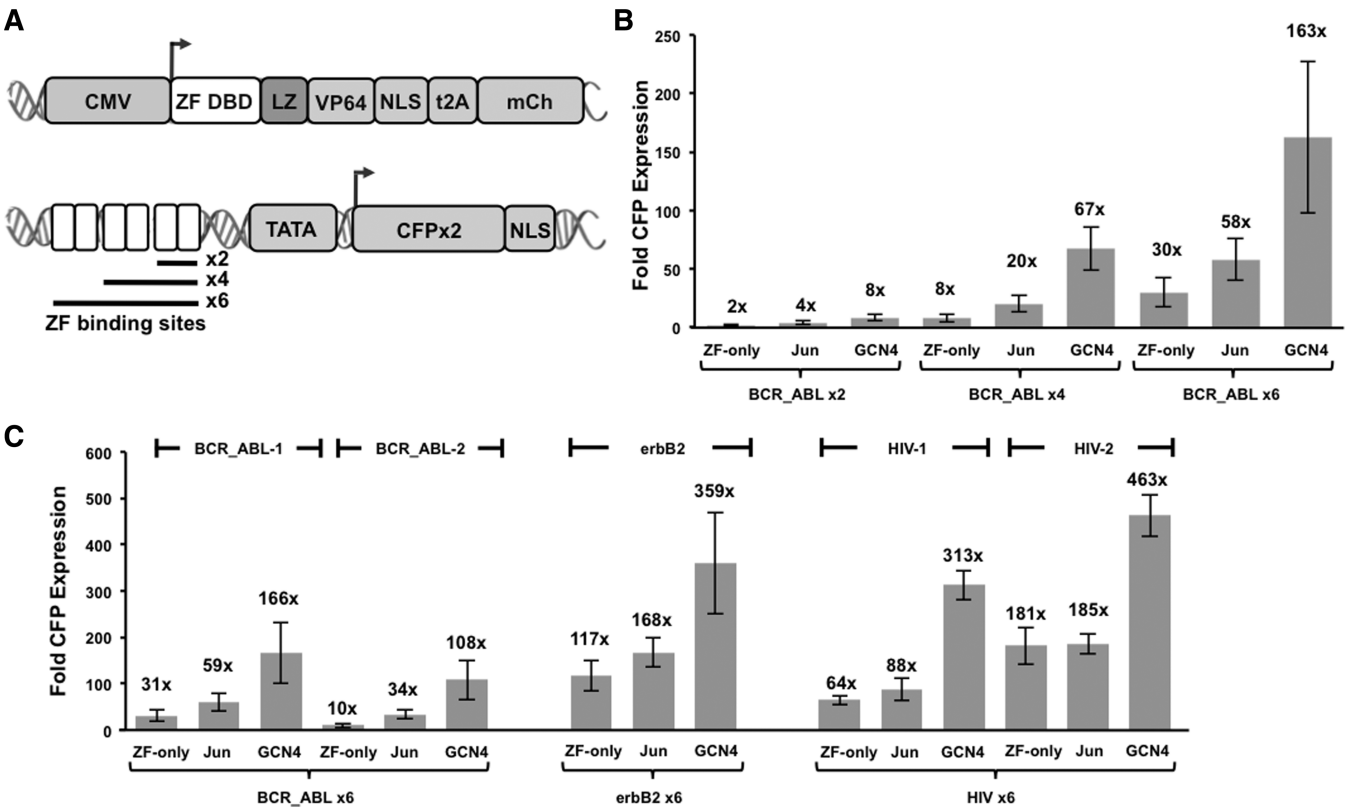

Figure 1. Engineering and characterization of ZF transcriptional activators. (**A**) Schematic representation of the assay used to test ZF activator function. Each transcriptional activator is expressed from the CMV promoter and tagged with a co-translationally cleaved t2a:mCherry fluorescent protein to monitor expression. ZF activator function is measured by the ability to activate the expression of 2 fused copies of cyan fluorescent protein from a reporter containing a minimal promoter and a variable number of 9 bp ZF target sites. (**B**) Characterization of the role of leucine zipper addition and target site copy number on ZF-TF transcriptional activation. BCR_ABL-1 activators fused to either no LZ (ZF-only), the c-Jun LZ (Jun), or the GCN4 LZ (GCN4) were co-transfected into U-2 OS cells along with reporter plasmids containing either 2, 4 or 6 copies of the corresponding 9 bp target site. CFP reporter expression as measured by flow cytometry and expressed as fold change over an off-target expression control. (**C**) Functional characterization of all ZF-activators co-transfected with reporter plasmids containing 6 copies of their 9 bp target sites.

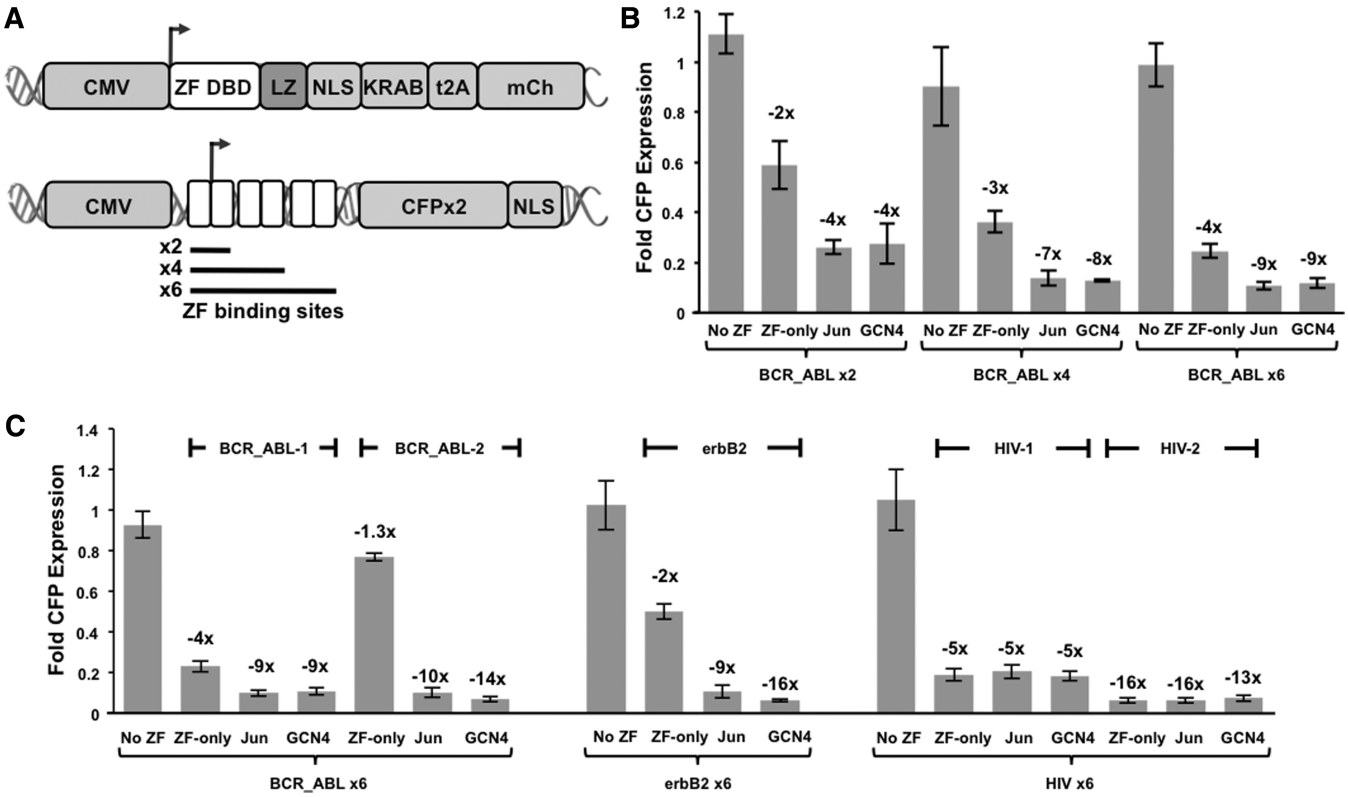

Figure 2. Engineering and characterization of ZF transcriptional repressors. (**A**) Schematic representation of the assay used to test ZF repressor function. Each transcriptional repressor is expressed from the CMV promoter and tagged with a co-translationally cleaved t2a:mCherry fluorescent protein to monitor expression. ZF repressor function is measured by the expression of 2 fused copies of cyan fluorescent protein from a CMV promoter engineered to have a variable number of 9 bp ZF target sites inserted into the transcriptional start site. (**B**) Functional characterization of the role of target site copy number and leucine zipper addition on ZF repressor activity. BCR_ABL-1 activators fused to either no LZ (ZF-only), the c-Jun LZ (Jun), or the GCN4 LZ (GCN4) were co-transfected into U-2 OS cells along with reporter plasmids containing either 2, 4 or 6 copies of the corresponding 9 bp target site. The activity of each ZF repressor was determined by CFP expression measured by flow cytometry and expressed as fold change over an off-target expression control. (**C**) Functional characterization of all ZF-repressors co-transfected with reporter plasmids containing 6 copies of their 9 bp target sites.

Figure S7). The HIV repressors were the only exception displaying no LZ-mediated increase. As expected, no repression was seen for off-target reporters (Supplementary Figures S8 and S9).

ZF-based Boolean logic computation

Using this set of synthetic ZF-TFs, we next sought to construct a set of Boolean logic gates. We divided the logic architecture into three general components: (i) a sensory module that senses inputs and converts the signals into ZF expression, (ii) a computational module comprised of ZFs and corresponding response promoters and (iii) an output module consisting of a gene encoding a given protein.

Within this framework, we began by generating response constructs that exhibited OR gate behavior. OR gates were developed by utilizing hybrid promoters consisting of various copies of binding sites for two distinct ZF DBDs. To determine the effect of binding site architecture on signal output, constructs containing either 2, 4 or 6 copies of the BCR_ABL and erbB2 binding sites were generated in multiple configurations (Figure 3A and Supplementary Figures S10 and S11). We characterize all of our Boolean logic systems using artificial inputs in which the CMV promoter drives expression of the computational proteins for a positive input or a negative control protein for a negative input. Each OR gate configuration was tested by co-transfection with either the BCR_ABL-1:GCN4 activator, the erbB2:Jun activator or both activators in tandem. All promoter architectures functioned as OR gates, with either a single activator alone or both factors present together resulting in signal output. The presence of both activators in tandem resulted in an additional 7-fold increase in output signal, likely due to the increased occupancy of reporter target sites by the transcriptional activators (Figure 3A). We also observed minor position effects, with activator constructs having corresponding binding sites more proximal to the TATA box displaying higher induction (Supplementary Figures S10 and S11). The varying outputs for different promoter architectures allow for an additional potential layer of tunability.

A similar approach was employed using ZF repressors to compute NOR logic. As with our OR gates, NOR gates were generated by placing binding sites for two different ZFs within the repressor reporter plasmids. Reporters were constructed with either 2, 4 or 6 binding sites in multiple configurations, and tested by transfecting with

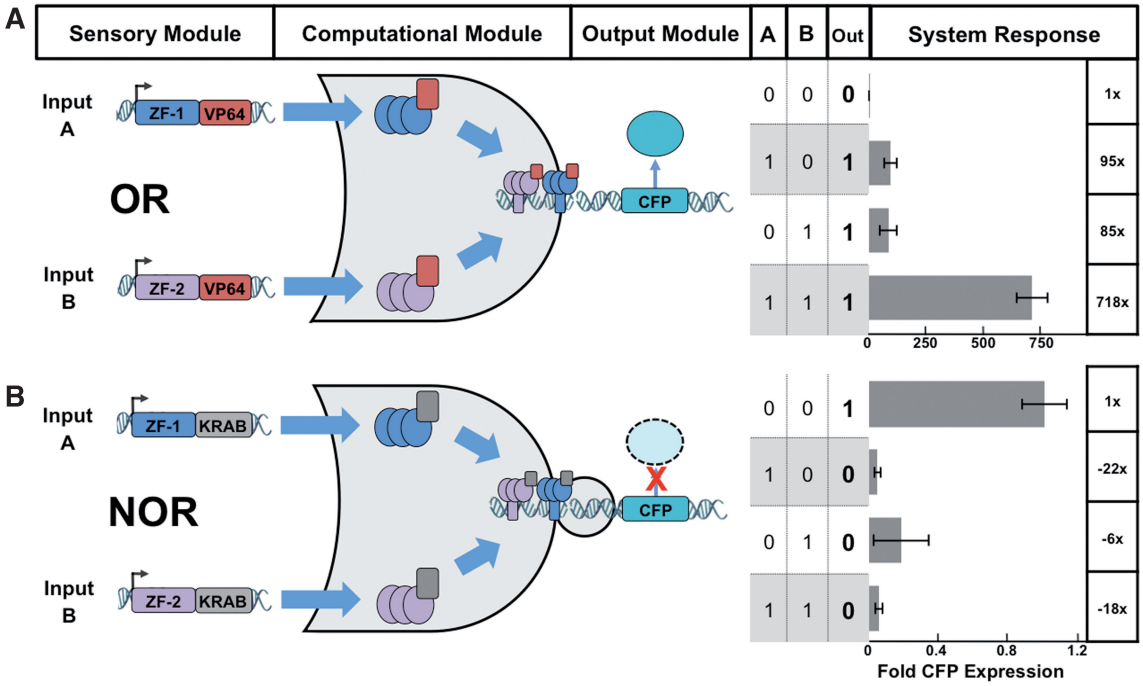

Figure 3. Engineering and characterization of ZF-based OR and NOR Boolean logic gates. In the sensory module, input signals lead to expression of corresponding ZF-based transcription factors. In the computational module, transcription factors act on response promoters. (**A**) OR gate response promoters contain target sites for two different ZF activators, and the logical operation is computed as TRUE (CFP expression) when either one or both inputs is present. For the response data shown BCR_ABL-1:GCN4 and erbB2:Jun activators were used as ZF-1 and ZF-2, respectively, and the response promoter contains six copies of the BCR_ABL target site upstream of 6 copies of the erbB2 target site. CFP expression was measured by flow cytometry and expressed as fold change over an off-target expression control. (**B**) NOR gate response promoters contain the binding sites for two different ZF repressors, and the logical operation is computed as TRUE when neither input is present. For the response data shown BCR_ABL-1:GCN4 and erbB2:Jun repressors were used as ZF-1 and ZF-2, respectively, and the response promoter contains six copies of the BCR_ABL target site upstream of 6 copies of the erbB2 target site. CFP expression was measured by flow cytometry and expressed as fold change over an off-target expression control.

either the BCR_ABL-1:GCN4 repressor, the erbB2:Jun repressor or both repressors. All promoter architectures functioned as NOR gates, with repression levels ranging from 2- to 23-fold. We again observed a minor position effect with higher levels of repression corresponding to ZF binding site proximity to the CMV TATA box. Thus, NOR gates can also be tuned to have different response properties (Figure 3B and Supplementary Figures S12 and S13).

We next sought to compute AND and NAND logic using our transcriptional activators and repressors. To use our split intein protein splicing strategy, we first set out to determine the optimal amino acid residue at which to split our ZF-TFs. We created twelve pairs of BCR_ABL-1:Jun activator split proteins. Each pair contained an amino- (N-) and carboxy-terminal (C-) fragment fused to the appropriate intein. These fragments were co-transfected, either together or separately, with the 6× BCR_ABL activator reporter (Figure 4A, B and C). Fold induction was calculated relative to CFP activation by the C-terminal fragment alone. Five out of twelve ZF split pairs displayed >3-fold signal output (Figure 4D and Supplementary Figure S14). The split site between residues 30 and 31 resulted in the highest activity, ~19-fold, and was therefore chosen for further logic gate generation. Interestingly, all functional split sites are predicted to be located in protein loop regions of the ZF, suggesting the importance of the secondary structure on efficient protein splicing (Supplementary Figure S15). After performing this assay we discovered that a truncated form of the N-terminal intein fragment, intN*, lacking four C-terminal amino acids displayed higher splicing efficiency, and we used this intein fragment in all further experiments.

Next, we generated an AND gate using split BCR_ABL-1:GCN4. Cells were transfected with each fragment alone or both fragments together, and an off-target ZF DBD was used as a negative control. When both N-terminal and C-terminal fragments of BCR_ABL-1:GCN4 activator were present, we observed a 154-fold signal induction, a level that is comparable with that of the parental BCR_ABL-1:GCN4 activator (Figure 5A and Supplementary Figure S16). A NAND gate or 'NOT AND' gate is the opposite of an AND gate, returning 'TRUE' as long as both inputs are not present together. To compute NAND logic, we sought to splice together fragments of the BCR_ABL-1:GCN4 repressor. The repressor was split in the same location as the BCR_ABL activators. We assayed for NAND activity by co-transfection of the 6× BCR_ABL repressor reporter with either fragment alone or both fragments together. No repression was seen when either the N-terminal or C-terminal fragment was transfected alone, and when both fragments were present, a 3-fold repression was observed (Figure 5B and Supplementary Figure S17).

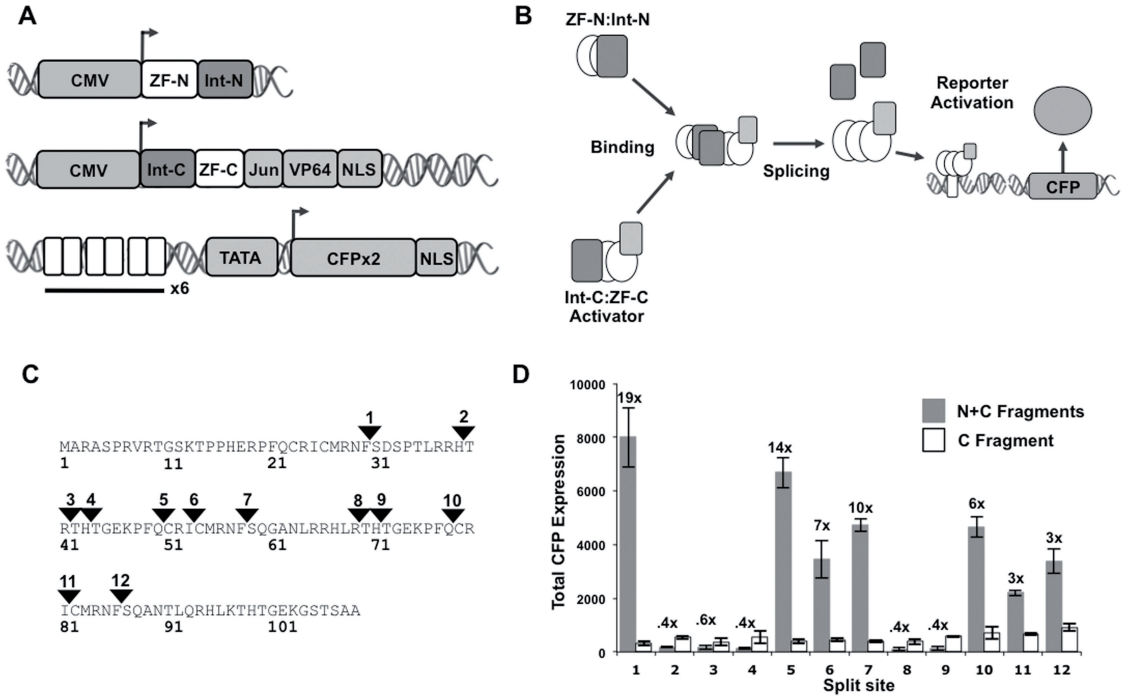

Figure 4. Determining the optimal ZF-TF split site. (**A**) Schematic representation of the plasmids used to test for split ZF activator function. Each ZF-N:int-N or Int-C:ZF-C fragment is expressed from a CMV expression plasmid. Activity is measured by the ability of each fragment pair to activate a cyan fluorescent protein reporter containing 6 copies of 9 bp ZF target sites versus activation by the Int-C:ZF-C fragment alone. (**B**) Schematic of the ZF-TF reconstitution process. After expression, the two split ZF-intein fragments bind together and undergo protein splicing to cleave away intein fragments and reconstitute the full ZF activator leading to activation of the BCR_ABL reporter. (**C**) BCR_ABL-1 amino acid sequence labeled with the 12 split sites assayed. (**D**) Characterization of the 12 ZF-intein activator pairs assayed by transient transfection in U-2 OS cells. CFP reporter expression was measured by flow cytometry and reported as total CFP expression. Fold changes in total CFP are listed for the activation of each split pair compared with activation by the corresponding Int-C:ZF-C fragment alone.

DISCUSSION

We developed a large set of tunable ZF-TF computing elements and general transcriptional framework to perform Boolean logic operations in mammalian cells. ZF-TFs present a scalable alternative to common synthetic biology transcriptional regulators such as LacI, Gal4 and TetR with >100 ZF DBDs that target mutually orthogonal DNA sequences available (7,8). We created activators and repressors using five previously developed ZF DBDs that target three orthogonal 9 bp DNA sequences and corresponding response promoters. As these ZF DBDs are highly similar in structure to other artificial ZF DBDs, it is likely that these too can be readily integrated into our system architectures. In order to generate system components that interrogate signals of different strengths and yield responses of different strengths, we developed methods to tune ZF-TFs. We employed two general strategies borrowed from naturally occurring systems: fusing ZF-TFs to LZ homodimerization domains and altering the number of ZF binding sites in response promoters. We created a large set of parts and elucidated general design rules based on the behaviors of these parts. Activators displayed an increase in activity correlating with both the number of promoter binding sites and the strength of the LZ interaction domain. The repressors behaved similarly displaying an increase in repression corresponding to the number of binding sites and the presence of a LZ. Whereas the strength of the LZ domain did not impact the repression levels, this could be the result of weaker repressors reaching a maximum repression level for the transient transfection repressor assay. Both tuning methods could be employed together to obtain maximum ZF-TF activity levels. The identity of the ZF DBD also affected ZF-TF activity, potentially due to differences in DNA binding strength or subtle differences in ZF-TF expression levels. This element provides yet another way to tune ZF-TF. Whereas the precise mechanism of LZ-enhanced ZF-TF activity is unclear, we speculate that it could be the result of cooperative transcription factor binding or LZ-mediated recruitment of additional ZF-TFs to the promoter region. Both mechanisms would lead to increased promoter occupancy by the ZF-TFs and a corresponding increase in activity.

To integrate signals for logic computations, we employed hybrid promoter and novel split intein protein splicing integration architectures. We observed strong ON/OFF ratios for idealized CMV-expressed inputs for OR, NOR, AND and NAND gates. The hybrid promoter strategy used for OR and NOR computations effectively integrated ZF-TF signals and showed tunability dependent on ZF binding site number and LZ strength. Whereas all inductions were high, the OR gate behavior was somewhat analog as the presence of two inputs showed

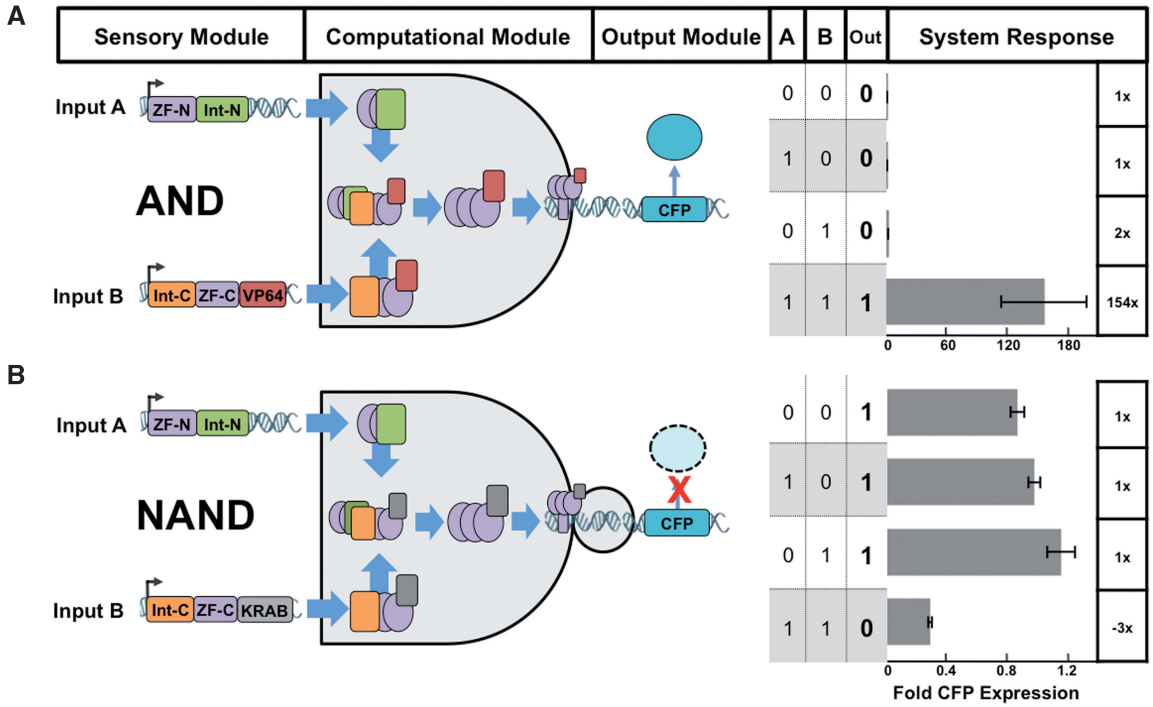

Figure 5. Engineering and characterization of ZF-based AND and NAND Boolean logic gates. In the sensory module, the presence of an input signal leads to the expression of the corresponding ZF-TF:split intein fragment, either ZF-N:Int-N or Int-C:ZF-C. In the computation module splicing of ZF:intein fragments leads to production of a complete ZF-TF that acts upon its cognate promoter. (**A**) For AND gates, a ZF activator is spliced and the logical operation is computed as TRUE only when both input signals are present. For the response data shown BCR_ABL-1:GCN4 activator split fragments were used and the response promoter contains 6 copies of the BCR_ABL target site. CFP expression was measured by flow cytometry and expressed as fold change over an off-target expression control. (**B**) For NAND gates, the computational module splices a ZF repressor, and the logical operation is computed as TRUE as long as both inputs are not present together. For the response data shown BCR_ABL-1:GCN4 repressor split fragments were used and the response promoter contains 6 copies of the BCR_ABL target site. CFP expression was measured by flow cytometry and expressed as fold change over an off-target expression control.

a 7-fold increase over the presence of each single input. Interestingly, this result suggests that the individual ZF-TF response promoters could perhaps be further enhanced by the addition of more ZF binding sites beyond the 6× BS systems we report in Figure 1. The position of the ZF binding sites also affected OR gate activity with higher activation levels observed from ZF-TFs with binding sites closer to the TATA Box. The NOR gates showed comparable repression levels for single and double inputs but also displayed a position effect with stronger repression levels observed for ZF binding sites located directly on the putative transcription start sites.

To compute AND and NAND logic we combined split intein protein splicing with our ZF-TF components. Protein splicing provides a novel method to efficiently combine signals that has the advantage of generating fully formed transcription factors. We first found the optimal split site for the ZF-TF activators among 12 putative split sites assayed. Interestingly, 7 out of 12 split sites were successful at activating reporter function >3-fold demonstrating the modularity of the split inteins. All successful split sites were located in protein loop regions suggesting the importance of secondary structure on splicing efficiency. The most efficient split site showed activity levels matching that of the complete factor. As the split sites are located within the constant region of the BCR_ABL-1 ZF DBD it is likely they can be used in ZF-TFs containing different ZF DBDs. Finally, the optimal ZF split site was effective in the context of ZF activators with different LZ domains and also in the context of a repressor to perform NAND logic. The NAND gate showed around a 3-fold repression of the reporter. Whereas significantly lower than the complete factor (9-fold repression), this is possibly due to a delay caused by intein splicing that leads to expression from the CMV promoter before it can be efficiently repressed.

Together these system components greatly expand the repertoire of parts and devices available to mammalian synthetic biologists. The tuning methods were effective at generating a large variation in ZF-TF activities and could potentially be generalized to tune other transcription factors. While the reported systems can stand on their own, the parts and architectures could also be used in conjunction with other existing logic computational methods that rely on the use of synthetic transcription factors. While we characterize our systems using the transient transfection format, we expect that they should also function in the context of stable cell lines with qualitatively similar system behaviors. The logic framework developed utilizing these factors provides a powerful new and general method for computing Boolean logic in mammalian cells. Through the use of modular ZF DBDs and

LZ dimerization domains, we have developed an approach that should be readily scalable to different input/output requirements and tolerances. Components in the system, while orthogonal in specificity, share common structural and functional qualities, promising to make optimization of networks more streamlined and different networks more comparable. The potential modularity of cellular inputs and the tunability of output response within this framework lends itself to the processing of multiple cellular signals and the future rewiring of intrinsic network topologies to engineer precise biological responses. We envision using these system components to interrogate endogenous transcriptional inputs that are markers for cell type, cell state and other environmental stimuli. Future scaling up of these systems can follow our elucidated design principles and take advantage of the many additional LZs, ZF DBDs and split inteins available.

SUPPLEMENTARY DATA

Supplementary Data are available at NAR Online: Supplementary Tables 1–4, Supplementary Figures 1–17 and Supplementary References [22,23].

ACKNOWLEDGEMENTS

The authors wish to acknowledge M. Hoerner for technical assistance, as well as D. Burrill, M. Inniss, A. Garg and all members of the Silver lab for helpful comments and discussion. The authors would also like to acknowledge Y.P. Hung, D.B. Thompson, C.J. Delebecque and D. Burrill for carefully reading the manuscript.

FUNDING

NIH (grants 1F32 CA154195-01 to T.Z.A. and R37 GM36373-22 to P.A.S.); Wyss Institute for Biologically Inspired Engineering (to J.J.L. and P.A.S.) and DARPA (to P.A.S.). Funding for the open access charge: DARPA.

Conflict of interest statement. None declared.

REFERENCES

1. Kramer,B.P., Fischer,C. and Fussenegger,M. (2004) BioLogic gates enable logical transcription control in mammalian cells. *Biotechnol. Bioeng.*, **87**, 478–484.
2. Leisner,M., Bleris,L., Lohmueller,J., Xie,Z. and Benenson,Y. (2010) Rationally designed logic integration of regulatory signals in mammalian cells. *Nat. Nanotechnol.*, **5**, 666–670.
3. Rinaudo,K., Bleris,L., Maddamsetti,R., Subramanian,S., Weiss,R. and Benenson,Y. (2007) A universal RNAi-based logic evaluator that operates in mammalian cells. *Nat. Biotechnol.*, **25**, 795–801.
4. Win,M.N. and Smolke,C.D. (2008) Higher-order cellular information processing with synthetic RNA devices. *Science*, **322**, 456–460.
5. Xie,Z., Wroblewska,L., Prochazka,L., Weiss,R. and Benenson,Y. (2011) Multi-input RNAi-based logic circuit for identification of specific cancer cells. *Science*, **333**, 1307–1311.
6. Nissim,L. and Bar-Ziv,R.H. (2010) A tunable dual-promoter integrator for targeting of cancer cells. *Mol. Syst. Biol.*, **6**, 444.
7. Maeder,M.L., Thibodeau-Beganny,S., Osiak,A., Wright,D.A., Anthony,R.M., Eichtinger,M., Jiang,T., Foley,J.E., Winfrey,R.J., Townsend,J.A. *et al.* (2008) Rapid "open-source" engineering of customized zinc-finger nucleases for highly efficient gene modification. *Mol. Cell*, **31**, 294–301.
8. Sander,J.D., Dahlborg,E.J., Goodwin,M.J., Cade,L., Zhang,F., Cifuentes,D., Curtin,S.J., Blackburn,J.S., Thibodeau-Beganny,S., Qi,Y. *et al.* (2011) Selection-free zinc-finger-nuclease engineering by context-dependent assembly (CoDA). *Nat. Methods*, **8**, 67–69.
9. Hurt,J.A., Thibodeau,S.A., Hirsh,A.S., Pabo,C.O. and Joung,J.K. (2003) Highly specific zinc finger proteins obtained by directed domain shuffling and cell-based selection. *Proc. Natl Acad. Sci. USA*, **100**, 12271–12276.
10. Burz,D.S., Rivera-Pomar,R., Jäckle,H. and Hanes,S.D. (1998) Cooperative DNA-binding by Bicoid provides a mechanism for threshold-dependent gene activation in the Drosophila embryo. *EMBO J.*, **17**, 5998–6009.
11. Pomerantz,J.L., Wolfe,S.A. and Pabo,C.O. (1998) Structure-based design of a dimeric zinc finger protein. *Biochemistry*, **37**, 965–970.
12. Wolfe,S.A., Grant,R.A. and Pabo,C.O. (2003) Structure of a designed dimeric zinc finger protein bound to DNA. *Biochemistry*, **42**, 13401–13409.
13. Wolfe,S.A., Ramm,E.I. and Pabo,C.O. (2000) Combining structure-based design with phage display to create new Cys(2)His(2) zinc finger dimers. *Structure*, **8**, 739–750.
14. d'Avignon,D.A., Bretthorst,G.L., Holtzer,M.E., Schwarz,K.A., Angeletti,R.H., Mints,L. and Holtzer,A. (2006) Site-specific experiments on folding/unfolding of Jun coiled coils: thermodynamic and kinetic parameters from spin inversion transfer nuclear magnetic resonance at leucine-18. *Biopolymers*, **83**, 255–267.
15. Zitzewitz,J.A., Bilsel,O., Luo,J., Jones,B.E. and Matthews,C.R. (1995) Probing the folding mechanism of a leucine zipper peptide by stopped-flow circular dichroism spectroscopy. *Biochemistry*, **34**, 12812–12819.
16. Li,J., Sun,W., Wang,B., Xiao,X. and Liu,X.Q. (2008) Protein trans-splicing as a means for viral vector-mediated in vivo gene therapy. *Hum. Gene Ther.*, **19**, 958–964.
17. Liu,X.Q. and Hu,Z. (1997) A DnaB intein in *Rhodothermus marinus*: indication of recent intein homing across remotely related organisms. *Proc. Natl Acad. Sci. USA*, **94**, 7851–7856.
18. Perler,F.B. (2002) InBase: the Intein Database. *Nucleic Acids Res.*, **30**, 383–384.
19. Phillips,I. and Silver,P.A. (2006) A new biobrick assembly strategy designed for facile protein engineering. *DSpace*. MIT Artificial Intelligence Laboratory, MIT Synthetic Biology Working Group, Massachusetts Institute of Technology, Cambridge, MA.
20. Knight,T. (2003) Idempotent Vector Design for Standard Assembly of Biobricks. *DSpace*. MIT Artificial Intelligence Laboratory; MIT Synthetic Biology Working Group, Massachusetts Institute of Technology, Cambridge, MA.
21. Szymczak,A.L., Workman,C.J., Wang,Y., Vignali,K.M., Dilioglou,S., Vanin,E.F. and Vignali,D.A. (2004) Correction of multi-gene deficiency in vivo using a single 'self-cleaving' 2A peptide-based retroviral vector. *Nat. Biotechnol.*, **22**, 589–594.
22. Labarga,A., Valentin,F., Anderson,M. and Lopez,R. (2007) Web services at the European bioinformatics institute. *Nucleic Acids Res.*, **35**, W6–W11.
23. Elrod-Erickson,M., Benson,T.E. and Pabo,C.O. (1998) High-resolution structures of variant Zif268-DNA complexes: implications for understanding zinc finger-DNA recognition. *Structure*, **6**, 451–464.